AGU PUBLICATIONS

JGR

Journal of Geophysical Research: Atmospheres

RESEARCH ARTICLE
10.1002/2016JD026222

Key Points:
- Normalizing the water vapor isotope ratio with respect to water vapor concentration creates a new metric to track convective reorganization
- This new metric isolates isotopic variability caused by shifting imbalances between tropical precipitation and evaporation
- Since isotope ratios can be retrieved from remote sensing, variations in water cycle intensity can be investigated globally

Supporting Information:
- Supporting Information S1

Correspondence to:
A. Bailey,
adriana@dartmouth.edu

Citation:
Bailey, A., P. N. Blossey, D. Noone, J. Nusbaumer, and R. Wood (2017), Detecting shifts in tropical moisture imbalances with satellite-derived isotope ratios in water vapor, *J. Geophys. Res. Atmos.*, *122*, 5763–5779, doi:10.1002/2016JD026222.

Received 11 NOV 2016
Accepted 16 MAY 2017
Accepted article online 22 MAY 2017
Published online 10 JUN 2017

Detecting shifts in tropical moisture imbalances with satellite-derived isotope ratios in water vapor

A. Bailey[1,2], P. N. Blossey[3], D. Noone[4], J. Nusbaumer[5,6], and R. Wood[3]

[1]Joint Institute for the Study of the Atmosphere and Ocean, University of Washington, Seattle, Washington, USA, [2]Now at Department of Earth Sciences, Dartmouth College, Hanover, New Hampshire, USA, [3]Department of Atmospheric Sciences, University of Washington, Seattle, Washington, USA, [4]College of Earth, Ocean, and Atmospheric Sciences, Oregon State University, Corvallis, Oregon, USA, [5]Cooperative Institute for Research in Environmental Sciences and Department of Atmospheric and Oceanic Sciences, University of Colorado Boulder, Boulder, Colorado, USA, [6]Now at NASA Goddard Institute for Space Studies, New York, New York, USA

Abstract As global temperatures rise, regional differences in evaporation (*E*) and precipitation (*P*) are likely to become more disparate, causing the drier *E*-dominated regions of the tropics to become drier and the wetter *P*-dominated regions to become wetter. Models suggest that such intensification of the water cycle should already be taking place; however, quantitatively verifying these changes is complicated by inherent difficulties in measuring *E* and *P* with sufficient spatial coverage and resolution. This paper presents a new metric for tracking changes in regional moisture imbalances (e.g., *E-P*) by defining δD_q—the isotope ratio normalized to a reference water vapor concentration of 4 mmol mol^{-1}—and evaluates its efficacy using both remote sensing retrievals and climate model simulations in the tropics. By normalizing the isotope ratio with respect to water vapor concentration, δD_q isolates the portion of isotopic variability most closely associated with shifts between *E*- and *P*-dominated regimes. Composite differences in δD_q between cold and warm phases of El Niño–Southern Oscillation (ENSO) verify that δD_q effectively tracks changes in the hydrological cycle when large-scale convective reorganization takes place. Simulated δD_q also demonstrates sensitivity to shorter-term variability in *E-P* at most tropical locations. Since the isotopic signal of *E-P* in free tropospheric water vapor transfers to the isotope ratios of precipitation, multidecadal observations of both water vapor and precipitation isotope ratios should provide key evidence of changes in regional moisture imbalances now and in the future.

1. Introduction

Although there is a near-global balance in evaporation (*E*) and precipitation (*P*), there are regional differences that shape moisture transport globally. Moisture divergence balances these regional differences, so long as changes in moisture storage are negligible:

$$E - P = [\nabla \cdot \mathbf{Q}], \tag{1}$$

where the term on the right-hand side is the vertical integral of the moisture flux divergence—with **Q** defined as **V***q*—and is henceforth denoted [DIV] (Figure 1). Equation (1) illustrates why the subtropics, where $E > P$, export moisture to the equator and midlatitudes. As Earth warms, it is predicted that these regional moisture differences will become larger [e.g., *Held and Soden*, 2006].

In line with these predictions, remote sensing analyses suggest that precipitation has intensified in convective regions in the tropics [*Li et al.*, 2011; *Zhou et al.*, 2011]; however, estimates of *P* intensification depend strongly on both the data product and time period considered [*John et al.*, 2009]. Moreover, most studies ignore the smaller but possibly significant role that changes in evaporation play in determining the strength of net moisture export on a regional scale. In an effort to examine how spatial patterns of *E-P* are changing, *Durack et al.* [2012] used sea surface salinity records to investigate whether wet regions of the oceans are becoming fresher while dry regions are becoming more saline. Their analysis suggests that on average, regional moisture imbalances are intensifying at twice the rate predicted by thermodynamic models—a clear indication that no consensus exists on just how quickly the water cycle is responding to climate. An independent metric that can monitor imbalances between *E* and *P* and identify regional variations in net moisture export is therefore desirable.

This study evaluates the ability of the isotope ratio *D*/*H* (or ^{2}H/^{1}H) in water vapor to track shifting *E-P*—represented by variations in [DIV] (equation (1))—in the tropics. The investigation is motivated by the

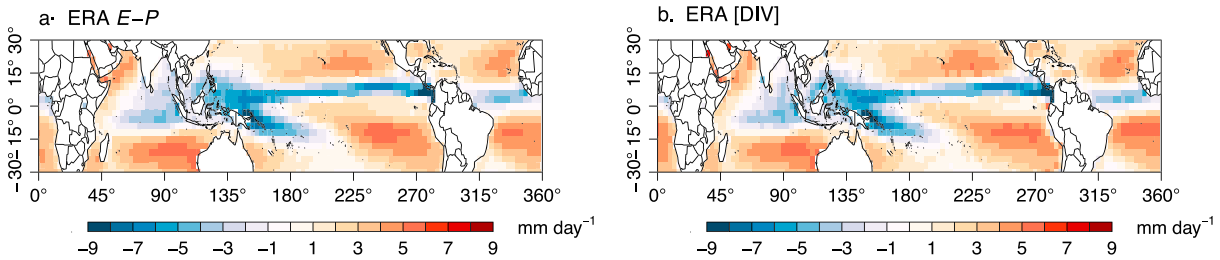

Figure 1. Mean patterns of (a) *E-P* and (b) [DIV] derived from daily mean estimates of these variables from the ERA-Interim reanalysis for the period September 2004 to December 2011.

fact that hydrogen isotope ratios are powerful tracers of water cycle processes due to their sensitivity to water phase changes. Because of their lower saturation vapor pressure, heavier isotopes (e.g., D or ^{2}H) preferentially condense and rain out, while lighter isotopes (e.g., ^{1}H) preferentially evaporate [*Dansgaard*, 1964]. Air masses recently moistened by evaporating surface waters are thus typically characterized by higher isotope ratios than air masses that have recently experienced condensation and precipitation [*Dansgaard*, 1964; *Gat*, 1996; *Noone*, 2012; *Brown et al.*, 2013].

More important, however, is the fact that for a given humidity, the isotopic composition of an air mass depends on the process by which it is moistened or dehydrated. Figure 2 illustrates this point by showing the dependence of the isotope ratio ($R = D/^1$H) on water vapor volume mixing ratio (q) for two irreversible processes, which span the majority of water isotopic observations globally [*Worden et al.*, 2007; *Lee et al.*, 2011; *Noone*, 2012]. Note that here and throughout the paper, isotope ratios are expressed in delta notation: $\delta D = (R/R_{\mathrm{VSMOW}} - 1) \times 1000$, where R_{VSMOW} is the isotope ratio of Vienna Standard Mean Ocean Water. The solid red line in Figure 2 shows the isotopic variation of an air mass experiencing moisture loss through precipitation. Since the precipitation process is assumed to be 100% efficient, the isotopic evolution of the air mass is described by a Rayleigh distillation model [*Dansgaard*, 1964]:

$$R = R_0 (q/q_0)^{\alpha - 1}, \tag{2}$$

where 0 represents a reference level (e.g., the lifting condensation level), and α is a temperature-dependent fractionation factor defined by the ratio of saturation vapor pressures for the H_2O and HDO isotopologues. The solid blue line, in contrast, shows the isotopic variation of the same air mass were it to become diluted through mixing with the dry free troposphere.

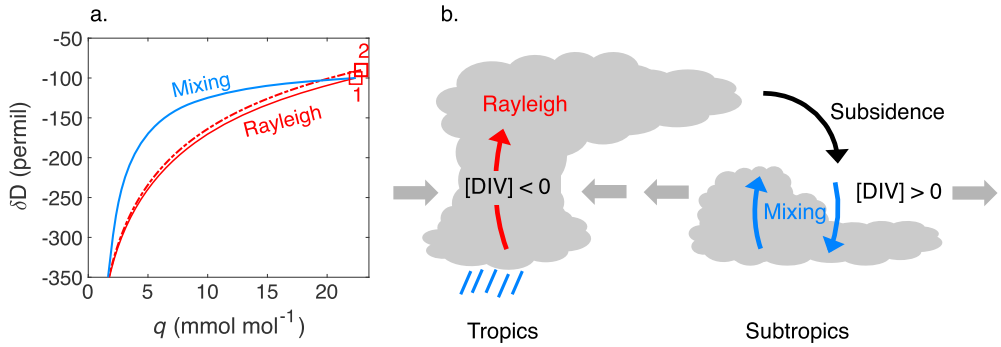

Figure 2. (a) Hypothetical variations in the isotope ratio (δD) as a function of the water vapor volume mixing ratio (q). The open square labeled "1" ($\delta D = -100‰$, $q = 22$ mmol mol^{-1} and $T = 290$ K at the lifting condensation level) shows the departure point for two processes: Rayleigh distillation of an air mass (solid red line) and mixing between that air parcel and a hypothetical free tropospheric air mass with $\delta D = -400‰$ and $q = 1.4$ mmol mol^{-1} (solid blue line). The dashed red line represents a Rayleigh distillation process for an air mass hypothetically originating from a region of warmer SST (open square "2," $\delta D = -90‰$ and $q = 23$ mmol mol^{-1} at a lifting condensation level defined by $T = 290$ K). The δD, q, and T values of these reference air masses are based on representative values observed by *Bailey et al.* [2015] near Hawaii, U.S. (b) A schematic representation of Rayleigh (i.e., precipitation) and mixing processes in tropical environments and their relationship with vertically integrated moisture flux divergence ([DIV]).

Together, these Rayleigh (red) and mixing (blue) curves approximate the hydrological cycle. In deep convective regions of the tropics, precipitation exceeds evaporation and dehydrates the atmosphere (solid red line), requiring that a net import, or convergence, of moisture take place (equation (1)). Air masses detrained from deep convective regions then subside until they are entrained into cloud-topped boundary layers in the subtropics and remoistened through mixing (solid blue line). The combined large-scale subsidence and mean tendency for E to exceed P in the subtropics result in a net export, or divergence, of moisture (equation (1)). What Figure 2 thus demonstrates is that variations in the isotope ratio around a fixed water vapor concentration (q) should distinguish E- and P-dominated environments.

Previous studies provide additional evidence that this should indeed be the case. *Lee et al*. [2007], for example, argued that both water vapor and precipitation will become enriched in heavy isotopes as $(E - P)/P$—and the relative contribution of local (versus imported) moisture to precipitation—increases. They found that this relationship explained climatological patterns in an isotopically enabled version of the Community Atmosphere Model version 2 (CAM2) and in precipitation observations collected throughout the tropics. *Moore et al*. [2014] found a similar relationship in idealized cloud-resolving simulations of tropical deep convection. These studies improve upon the more traditional and probably oversimplistic view that variations in P alone are what drive isotopic variability in the tropics [*Dansgaard*, 1964]—an assumption made by numerous paleoclimate analyses based on isotopic proxies recovered from tree rings, plant waxes, stalagmites, and sediment cores [e.g., *Cruz et al*., 2005; *Tierney et al*., 2008; *Niedermeyer et al*., 2010; *Sano et al*., 2012]. However, the ability of water vapor isotope ratios to track shifting regional moisture imbalances has yet to be evaluated systematically. This study leverages a record of isotopic retrievals from remote sensing that is nearly a decade long to investigate this relationship and to determine whether water vapor isotope ratios provide an independent assessment of hydrological changes on a near-global scale.

The study begins by defining δD_q, the hydrogen isotope ratio with respect to a fixed water vapor volume mixing ratio (q) of 4 mmol mol^{-1}. The first part of the analysis then evaluates tropical (30°S–30°N) spatial correlations between composite differences in δD_q—derived from NASA's satellite-borne Tropospheric Emission Spectrometer (TES)—and composite differences in E, P, and [DIV] from reanalysis. Composite differences are calculated for cold and warm phases of ENSO (El Niño–Southern Oscillation), which provides a natural test bed for evaluating isotopic responses to shifting regional moisture imbalances. Simulated δD_q from the National Center for Atmospheric Research (NCAR)'s isotope-enabled Community Atmosphere Model version 5 (iCAM5) is examined in a corollary analysis to provide insight where satellite coverage is sparse. While the analysis shows that convective reorganization during ENSO drives large and significant spatial variations in both P and [DIV], it is the latter that appears most strongly correlated with δD_q.

The second part of the analysis investigates whether variations in δD_q with ENSO are indeed a response to—and not simply a correlate of—the changes in [DIV] observed. Two sensitivity tests are carried out. In the first test, composite differences in δD_q are constructed for periods of low and high [DIV], which are defined over the entire analysis period: September 2004 to December 2011. In the second test, the simulated δD_q composite differences are reanalyzed holding precipitation approximately fixed. The results suggest that δD_q traces variability in E-P—and not just P—regardless of the strength or phase of ENSO. Since the δD_q signature in water vapor is transferred to condensate and rain, it is thus expected that long-term measurements of isotope ratios in both water vapor and precipitation should provide an important signal of changes in the atmospheric hydrological cycle with climate variations.

2. Methods

2.1. Defining δD_q From Remote Sensing and Climate Model Simulations

As illustrated in Figure 2, variations in the isotope ratio around a fixed water vapor concentration distinguish E- and P-dominated regimes. To isolate this isotopic variability, we define δD_q as the isotope ratio of hydrogen at a water vapor volume mixing ratio (q) of 4 mmol mol^{-1}. Although atmospheric q is seldom 4 mmol mol^{-1}, it is nevertheless a useful reference humidity since satellite-borne instrumentation is particularly sensitive to isotopic differences between Rayleigh- and mixing-like states at this humidity level [*Bailey*, 2014]. Furthermore, in many locations, 4 mmol mol^{-1} falls within a broad swath of the lower-to-middle free troposphere that explains much of the variance in total column water—a strong predictor of deep convective development and precipitation [*Holloway and Neelin*, 2009]. Nevertheless, the exact value of 4 mmol mol^{-1} is arbitrary.

For this study, observationally based estimates of δD_q are derived from jointly retrieved HDO and H_2O volume mixing ratio (i.e., q) profiles from NASA's Tropospheric Emission Spectrometer (TES) Lite version 6 data set [*TES Science Team*, 2013]. Model-based estimates are derived from daily mean vertical profiles of HDO and H_2O simulated by the isotopically enabled version of NCAR's Community Atmosphere Model version 5 (iCAM5, hereafter simply denoted "CAM") [*Nusbaumer et al*., 2017]. The model outputs come from a free-running CAM simulation forced by observed sea surface temperatures (SSTs) over the years 1995–2014, with a horizontal resolution of 1.9°N × 2.5°E. Although *Nusbaumer et al*. [2017] used the full TES averaging kernel to validate the model's performance, the present study does not adjust the CAM output in this manner. Nor does it filter the CAM daily output by cloud fraction. While these decisions may limit comparability between the CAM and TES isotopic information presented, they facilitate identification of isotopic variations that may be masked due to the limited vertical resolution and spatiotemporal coverage of the remote sensing observations.

TES is an infrared spectrometer that flies aboard the Aura spacecraft as part of NASA's A-Train satellite constellation. The analysis uses retrievals from the nadir-viewing mode, which has a horizontal footprint of 5.3 km × 8.3 km. TES Lite products, which are available online from NASA's Atmospheric Science Data Center (https://eosweb.larc.nasa.gov/) [TES Science Team, 2013], come corrected for known isotopic biases, which are discussed in *Worden et al*. [2011, 2012]. HDO and H_2O volume mixing ratios are provided for 17 pressure levels; however, the degrees of freedom associated with the HDO profile are typically close to 1. While data coverage spans September 2004 to the present, spatiotemporal coverage becomes very sparse in the later years. As a result, the analysis focuses on the September 2004 to December 2011 period, which includes the years with greatest global coverage, as well as two El Niño winters (2006–2007 and 2009–2010) and two La Niña winters (2007–2008 and 2010–2011).

Two filters are applied when selecting TES HDO profiles to ensure high quality data. First, only profiles with at least 0.5 degrees of freedom in HDO are selected to ensure that the final retrieval is not excessively biased by a priori assumptions about the true atmospheric state [e.g., *Worden et al*., 2007; *Noone*, 2012; *Brown et al*., 2013]. Second, because the sensitivity of the retrieval to the true atmospheric state diminishes while simultaneously shifting upward as cloudiness increases [*Lee et al*., 2011], only those retrievals with an average cloud optical depth (COD) less than 3.6 are used. *Lee et al*. [2011] showed that the shape and magnitude of the averaging kernel are comparable for retrievals in clear sky (e.g., COD less than 0.2) and non–precipitating-cloud conditions (e.g., COD greater than 0.2 and less than 3.6). Nevertheless, stricter cloud filters are tested and discussed as part of the supporting information. Importantly, isotope ratios measured under nonprecipitating conditions still reveal information about precipitation processes occurring close in space and/or time [*Gat*, 1996; *Worden et al*., 2007; *Brown et al*., 2008; *Noone*, 2012]. This is due to the fact that barring atmospheric mixing, to first order the isotopic composition of an air mass is set by condensation processes that occurred at the point of last saturation [*Hurley et al*., 2012].

Before the isotope ratio at $q = 4$ mmol mol^{-1} is predicted, the TES HDO and H_2O profiles from each 24 h period are averaged to a 3° × 3° grid matching the gridded product from the ECMWF (European Centre for Medium-Range Weather Forecasts) ERA-Interim reanalysis [*Dee et al*., 2011]. Similarly, the daily mean simulated profiles from CAM are interpolated to the ERA grid using nearest neighbor weighting. The quantity δD_q is estimated by regressing the vertical profile of the HDO volume mixing ratio against the vertical profile of the H_2O volume mixing ratio and predicting the HDO concentration at 4 mmol mol^{-1}. Unlike the actual isotope ratio, the HDO volume mixing ratio varies approximately linearly with the H_2O volume mixing ratio, allowing a simple linear regression to suffice for this purpose. The HDO concentration is subsequently converted to an isotope ratio and expressed in delta notation. To eliminate a small number of outliers whose values lie outside the expected range of lower and midtropospheric hydrogen isotope ratios in the Pacific [e.g., *Worden et al*., 2011; *Bailey et al*., 2013], the top and bottom percentile of TES δD_q are excluded from the analysis. These outliers are the result of poor regression fits between the HDO and H_2O volume mixing ratio profiles.

Although δD_q bears resemblance to the metric $\Delta\delta D$ used by *Samuels-Crow et al*. [2014]—where $\Delta\delta D$ defines the difference between the isotope ratio estimated from satellite and the isotope ratio predicted from a Rayleigh distillation (equation (2))—δD_q does not require one to make assumptions about the environment near cloud base. Similarities between these metrics are discussed in the supporting information.

2.2. Characterizing Shifts in Regional Moisture Imbalances Associated With ENSO

Variations in the spatial organization of convection caused by ENSO provide a natural test bed for investigating the sensitivity of δD_q to shifting regional moisture imbalances in *E* and *P*. For the purposes of this study, a composite warm phase (El Niño) is defined using the months September to February (SONDJF) from the years 2006–2007 and 2009–2010 and a composite cold phase (La Niña) is defined using the months SONDJF from the years 2007–2008 and 2010–2011. Differences between these two composites form the basis of the first part of the analysis. Shifts in the organization of convection between ENSO cold and warm phases are identified by evaluating composite differences in daily mean NOAA Interpolated OLR (Outgoing Longwave Radiation, provided by the NOAA/OAR/ESRL PSD, Boulder, Colorado, USA, from their Web site at http://www.esrl.noaa.gov/psd/) [*Liebmann and Smith*, 1996]; daily mean cloud top pressure from TES, filtered and regridded the same as the HDO profiles; daily mean cloud top pressure from the MODIS (Moderate Resolution Imaging Spectroradiometer) version 5 level 3 Aqua data set (available from https://ladsweb.nascom.nasa.gov/); and MODIS joint histograms of cloud optical depth and cloud top pressure. OLR anomalies are commonly used as a qualitative metric for describing the spatial reorganization of convection during ENSO [e.g., *Gill and Rasmusson*, 1983; *Rasmusson and Wallace*, 1983; *Lee et al*., 2015], even though no single threshold unambiguously distinguishes anomalies in convective activity [*Waliser et al*., 1993].

The effects of convective reorganization on regional moisture imbalances are demonstrated using composite differences in daily mean *E*, *P*, and [DIV] from ERA-Interim [*Dee et al*., 2011] and CAM, whose output is interpolated to the ERA 3° × 3° grid. Daily mean *E* and *P* from ERA are estimated by summing ECMWF's 12 h forecast accumulations of evaporation and precipitation, respectively, starting from the 0000 and 1200 UTC time steps. Daily mean [DIV]—which is assumed to represent *E-P* (equation (1), and see supporting information)—is estimated by averaging the instantaneous vertical integral of divergence of moisture flux from the 0000, 0600, 1200, and 1800 UTC time steps. In comparison, daily mean [DIV] from CAM is estimated for each grid using finite differences in spherical geometry:

$$[\mathrm{DIV}] = \frac{[uq]_{\lambda+} - [uq]_{\lambda-}}{2(\Delta x \cdot \cos\varphi)} + \frac{[vq]_{\varphi+} - [vq]_{\varphi-}}{2(\Delta y)}. \tag{3}$$

The first term differences the vertically integrated zonal moisture flux ([*uq*]) between the grid point to the east and the grid point to the west of the point of interest, while the second term differences the vertically integrated meridional moisture flux ([*vq*]) between the grid point to the north and the grid point to the south of the point of interest. Both terms are normalized by the distances over which the differences are calculated. The variables φ and λ are the latitude and longitude in radians, respectively, of the ERA 3° × 3° grid points, and Δx and Δy represent the lengths (m) of the two sides of a grid box at the equator.

2.3. Evaluating Isotopic Changes With Variations in *E-P*

To evaluate the sensitivity of water vapor isotope ratios to variations in regional moisture imbalances, the first part of the analysis examines spatial correlations between ENSO composite differences in daily mean δD_q and ENSO composite differences in *P*, *E*, and [DIV]. Composite differences in daily mean δD_z—which is here defined as the δD average for the 800–500-hPa layer of the atmosphere [cf. *Worden et al*., 2007; *Brown et al*., 2008; *Berkelhammer et al*., 2012]—and the δDs of total column condensate and precipitation in CAM are also examined. While the daily mean δD_z at each grid point is calculated as a mass-weighted average, the composite differences for both TES and CAM are derived from arithmetic temporal means. The δD of total column condensate is estimated for each grid point by vertically integrating the HDO and H_2O concentrations of liquid condensate and ice in CAM and weighting by the depth of each model pressure level.

The second part of the analysis performs a sensitivity test in which the strength of the spatial correlation between δD_q and [DIV] is evaluated over all months, irrespective of the strength or phase of ENSO. Its purpose is twofold: first, to assess whether variations in δD_q are indeed a response to shifting regional moisture imbalances between ENSO's cold and warm phases, and not simply a correlate, and, second, to examine more robustly the extent to which δD_q responds not just to *P* but to shifts in the balance between *E* and *P*. To accomplish these objectives, composite differences in observed and simulated δD_q are first calculated for periods of low and high [DIV], irrespective of the strength or phase of ENSO. So-called "low" and "high" periods are defined by the lower and upper [DIV] quartiles, respectively. The quartiles are computed from the

daily mean reanalysis and CAM output for the entire analysis period—September 2004 to December 2011—and for each grid point, to help normalize differences between regions characterized by strong moisture convergence (e.g., the Intertropical Convergence Zone (ITCZ), Figure 1b) and regions characterized by strong moisture divergence (e.g., the subtropics, Figure 1b). Second, the composite differences in simulated δD_q for periods of low and high [DIV] are further evaluated for the following narrow precipitation bins: 0–1 mm day^{-1}, 1–2.5 mm day^{-1}, 2.5–5 mm day^{-1}, and 5+ mm day^{-1}. It is expected that these low–high differences should capture variability in moisture transport on the time scales on which mesoscale features that induce convective activity exist. While the steady state assumptions of equation (1) may not be fully satisfied on these shorter time scales, the spatial dependence of δD_q on [DIV] is sufficiently similar to the spatial dependence of δD_q on *E-P* (Pearson correlation coefficient of 0.88) that only the former relationship is discussed in detail in the main text. Readers may refer to the supporting information for additional figures showing composite differences of δD_q for periods of low and high *E-P*.

2.4. Evaluating Significance Across Spatial Fields

Significant differences between cold and warm phases of ENSO and between low and high periods of [DIV] are evaluated at each grid point using a Welch two-sample *t* test. However, to limit false discoveries, the difference at a single location is only considered significant if its *p* value and all *p* values of equal or lesser value meet the criterion $p_i \leq (i/N)\alpha$, where *i* is the rank of the *p* value, *N* is the total number of finite-value local tests, and α is the significance level, which is set at 0.1 following the recommendation of *Wilks* [2016]. This choice of α most closely approximates a global significance level of 0.05. Significant differences in the reanalysis and model simulations that are detected by this method are represented in the figures with stippling. No stippling is shown for the satellite data due to the fact that limited temporal coverage results in few significant grid points. Differences are instead evaluated by averaging the TES results over much larger 15° × 25° areas.

3. Results

3.1. Large-Scale Convective Reorganization With ENSO

Between cold (La Niña) and warm (El Niño) phases of ENSO, the hydrological cycle reorganizes significantly, providing an ideal test bed for evaluating isotopic changes in water vapor in response to shifting regional moisture imbalances. Figure 3 shows the composite differences in OLR and cloud top pressure associated with the two La Niña and two El Niño events considered in this analysis. Although each individual phase of ENSO is unique, these composite differences reflect canonical patterns of convective reorganization [e.g., *Trenberth and Caron*, 2000]. For instance, during the La Niñas, changes in outgoing longwave radiation (OLR; Figure 3a) reflect a strengthening of convection in the Indo-Pacific Warm Pool (e.g., box 1, Figure 3), in subtropical regions east of Australia and near Hawaii (e.g., box 4, Figure 3), and, to a lesser degree, in the far eastern Pacific off the coasts of Ecuador and Peru (e.g., box 5, Figure 3). In comparison, during the El Niños, convective activity shifts toward the central Pacific (boxes 2 and 3, Figure 3) and strengthens eastward along the Intertropical Convergence Zone (ITCZ).

Composite differences in MODIS cloud top pressure confirm that decreases in OLR are linked to increases in cloud top height, associated with a deepening of convection (Figure 3b). The TES retrievals discern similar large-scale changes in cloud top pressure (Figure 3c), even though they are filtered for periods of low-fractional cloud cover. This finding suggests that despite neglecting cloudy scenes, the TES retrievals are sufficiently characteristic of the convective environments that define each ENSO phase.

Histograms of MODIS cloud top pressure versus cloud optical depth for liquid condensate (Figure 3e) provide a more detailed picture of the changes in cloudiness with height over the five boxed regions shown in Figures 3a–3d. While west of the dateline strengthening convective activity results in an increase in high clouds (boxes 1 and 2), east of the dateline it is midlevel clouds that increase (e.g., box 5); hence, reductions in OLR are not as great. Importantly, the pattern of these convective changes does not follow sea surface temperature (SST) changes exactly (Figure 3d), highlighting the importance of dynamical processes in altering moisture transport during El Niño and La Niña.

According to both reanalysis and CAM, changes in precipitation (ERA, Figure 4a; CAM, Figure 5a) broadly follow changes in convective activity and cloud top height as expected. Changes in vertically integrated

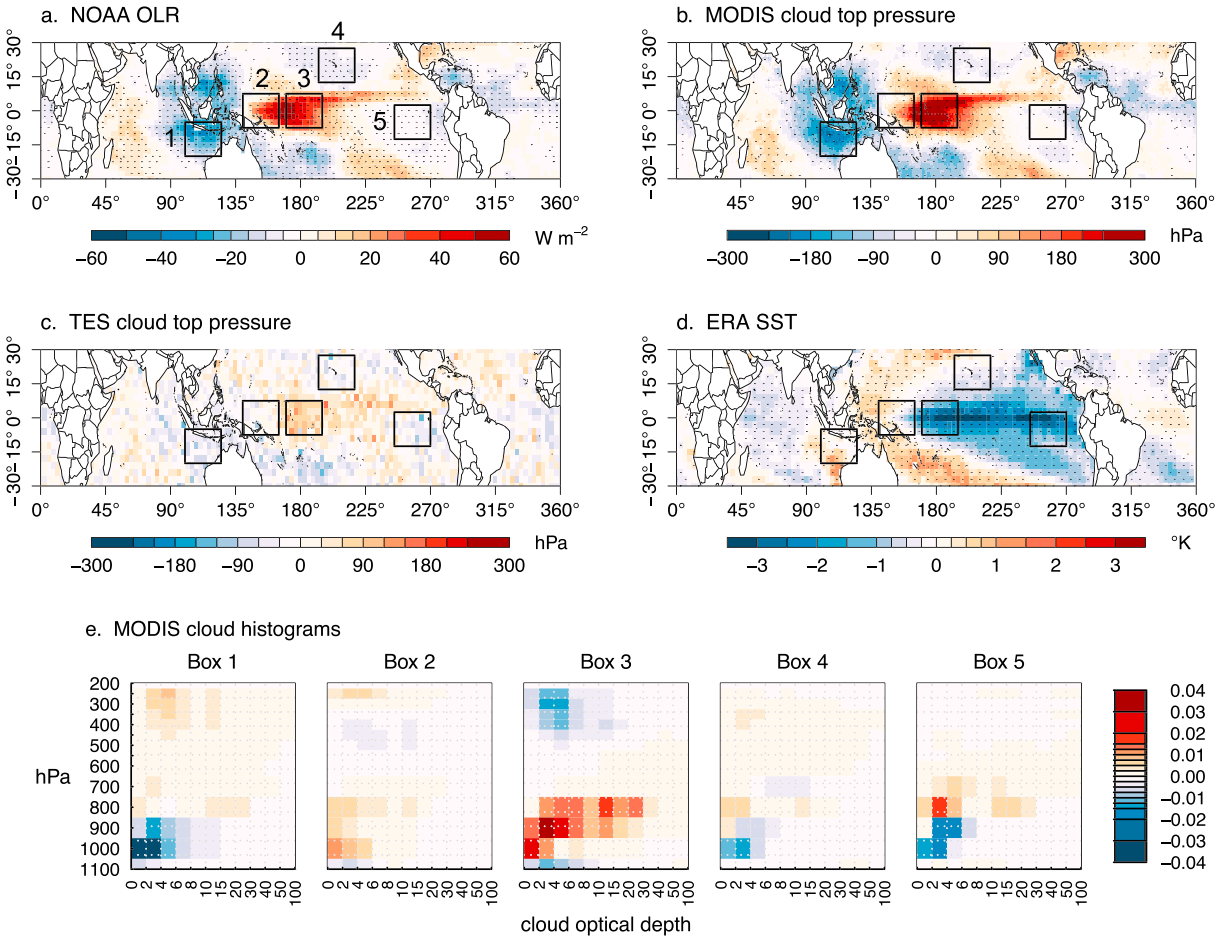

Figure 3. Changes in convective organization with ENSO. Composite differences in (a) NOAA OLR, (b) MODIS cloud top pressure, (c) TES cloud top pressure, and (d) ERA sea surface temperature (SST) for cold minus warm phases of ENSO. Stippling indicates significant differences. NOAA OLR and MODIS cloud top pressure are plotted on their native 2.5° × 2.5° and 1° × 1° grids, respectively; however, stippling in Figure 3b has been reduced to a 3° × 3° grid for clarity. (e) Composite differences in the MODIS joint histograms of cloud top pressure and cloud optical depth with ENSO are also shown for liquid cloud for the five boxed regions labeled in Figure 3a. Histograms for ice are qualitatively similar and thus not shown. The five boxed regions are each 15° × 25° in area, and their southwestern corners are defined by the following coordinates: (1) 20°S, 100°E; (2) 7.5°S, 140°E; (3) 7.5°S, 170°E; (4) 12.5°N, 192.5°E; and (5) 12.5°S, 245°E.

moisture flux convergence (the negative equivalent of the vertically integrated moisture flux divergence; ERA, Figure 4b; CAM, Figure 5b) are similar in pattern since the loss of atmospheric moisture through precipitation outpaces the increase in evaporative flux (ERA, Figure 4c; CAM, Figure 5c). In essence, transport must maintain the total column moisture necessary to sustain the observed increases in P in the absence of substantive changes in local E. Nevertheless, in some regions it is the changes in E that significantly alter the column-average hydrologic balance. In the east Pacific, for example, where changes in P are minimal (box 5, ERA, Figure 4a; CAM, Figure 5a), clear decreases in [DIV] are observed (ERA, Figure 4b; CAM, Figure 5b), consistent with a shift in E-P (ERA, Figure 4d; CAM, Figure 5d). Strong correlations (Pearson's $r > 0.97$) between the ENSO composite difference patterns of [DIV] (Figures 4b and 5b) and E-P (Figures 4d and 5d) support the interpretation that moisture transport balances local inequalities in E and P (equation (1)). A similar spatial pattern of isotopic changes would be expected if the water vapor isotope ratio is indeed a robust metric of E-P.

3.2. Isotopic Variations With Large-Scale Convective Reorganization

To evaluate the sensitivity of the water vapor isotope ratio to variations in E-P, composite differences in δD_q with ENSO are examined using both TES observations and CAM output.

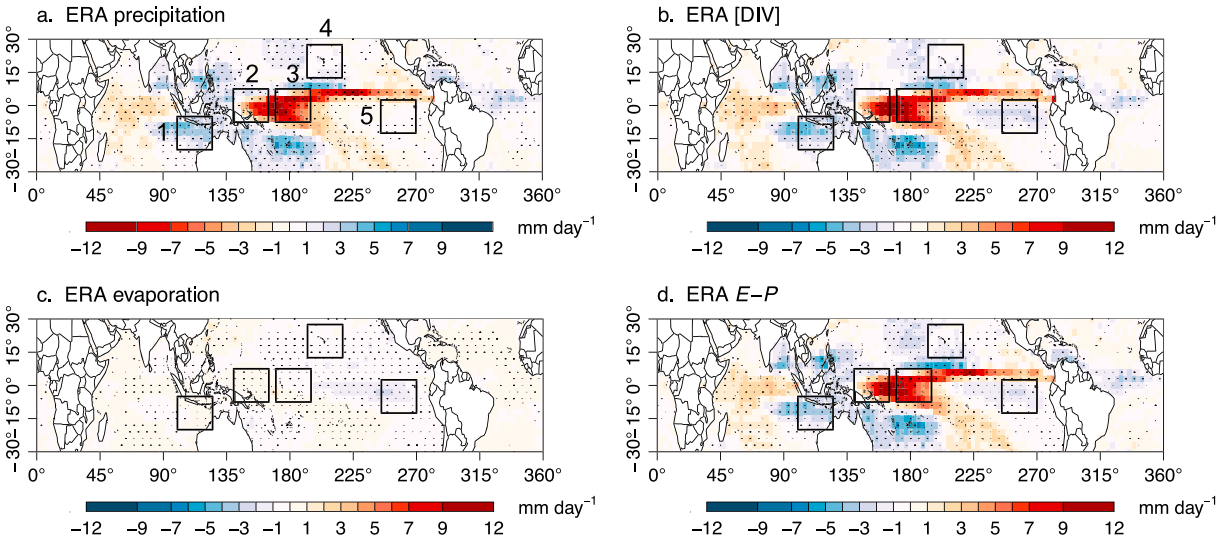

Figure 4. Changes in hydrologic balance with ENSO. Composite differences in (a) ERA precipitation, (b) ERA [DIV], (c) ERA evaporation, and (d) ERA *E-P* for cold minus warm phases of ENSO. Stippling indicates significant differences. The five boxed regions are the same as those shown in Figure 3 and discussed in the text.

As illustrated in Figures 6a and 6b, changes in δD_q closely follow the changes in convective reorganization with ENSO. This is particularly evident in CAM, where decreases in δD_q align with a deepening of convection (Figure 3a), an increase in *P* (Figure 5a), and a decrease in [DIV] (Figure 5b). A similar though noisier pattern is recognizable in the satellite observations, with the exception of the region marked by box 3. There the TES retrievals suggest that the δD_q response is variable even though CAM shows the expected positive correlation between δD_q and [DIV]. Interestingly, both TES and CAM identify decreases in δD_q in the east Pacific (box 5, Figure 7) where [DIV] decreases but *P* changes little—a finding that supports the hypothesis that δD_q is more sensitive to shifting regional moisture imbalances than to changes in *P* alone.

Revisiting Figure 2 allows us to interpret the information provided by the changes in δD_q with ENSO. The more δD_q decreases, the less hyperbolic and more logarithmic the relationship between the water vapor isotope ratio and volume mixing ratio presumably becomes. This shift from a more hyperbolic (e.g., "mixing" line) to a more logarithmic (e.g., "Rayleigh" line) curve in Figure 2 is consistent with a transition from a shallow

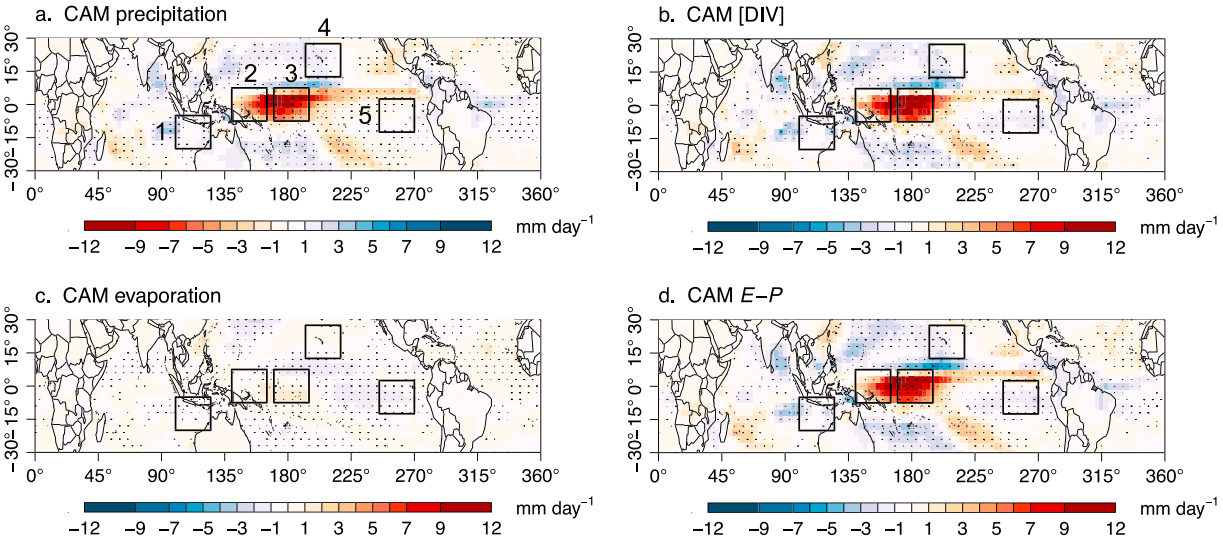

Figure 5. The same as Figure 4 but for CAM output.

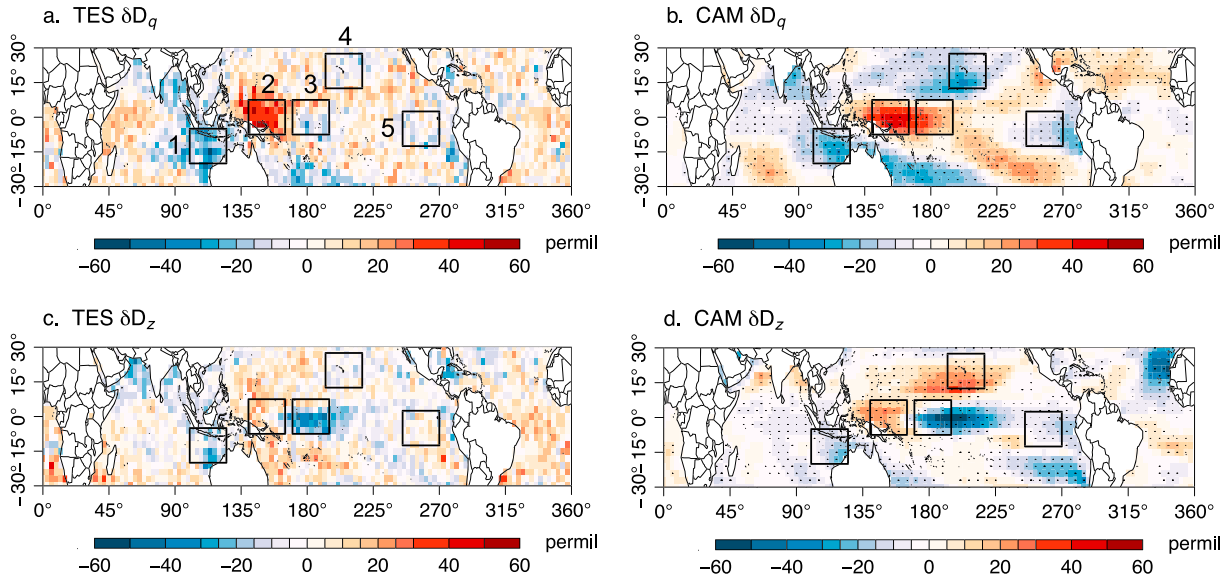

Figure 6. Changes in water vapor isotope ratios with ENSO. Composite differences in (a) TES δD_q, (b) CAM δD_q, (c) TES 800–500 hPa layer mean δD (δD_z), and (d) CAM δD_z for cold minus warm phases of ENSO. Stippling in Figures 6b and 6d indicates significant differences. The five boxed regions are the same as those shown in Figure 3 and discussed in the text.

convective environment, in which a temperature inversion separates the boundary layer and free troposphere, to a deeper convective environment, in which the atmosphere is closer in structure to a pseudoadiabat. The variations in δD_q with ENSO are thus not only correlated with but also theoretically consistent with the reorganization in convective activity observed.

In contrast, composite differences in the 800–500 hPa layer mean isotope ratio (e.g., δD_z, Figures 6c and 6d)—which is a much more traditional metric used for evaluating TES retrievals of water vapor isotope ratios [cf. *Worden et al.*, 2007; *Brown et al.*, 2008; *Berkelhammer et al.*, 2012]—are much less consistent with the patterns of convective reorganization. During La Niña, δD_z, like δD_q, decreases in the Indo-Pacific Warm Pool (e.g., box 1), albeit in a much less spatially coherent manner. However, δD_z also decreases over a large area of the central Pacific (e.g., box 3)—the location of greatest convective activity during the ENSO warm phase. Meanwhile, the simulations suggest that δD_z increases in the northern Pacific subtropics (e.g., box 4, Figure 6d), where [DIV] and δD_q decrease. These comparisons highlight the unique capability

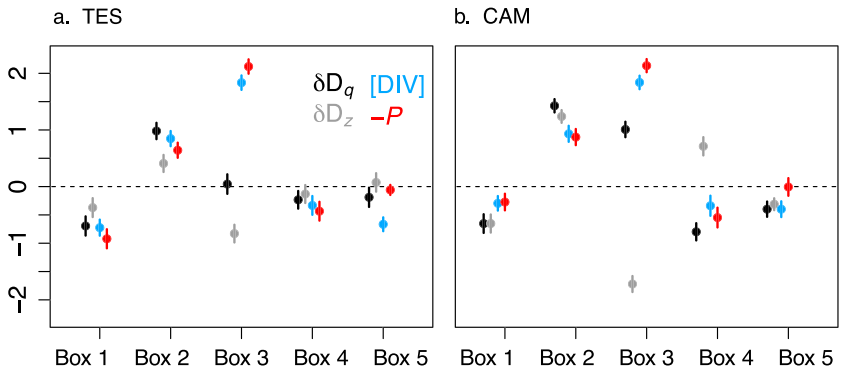

Figure 7. Mean normalized differences in δD_q (black), δD_z (gray), [DIV] (blue), and $-P$ (red) between cold and warm phases of ENSO for the five boxed regions in Figures 3–6. (a) Isotopic values from TES and estimates of [DIV] and $-P$ from ERA and (b) model-derived variables from CAM. Vertical lines represent 95% confidence intervals. Therefore, those points whose whiskers do not span zero are considered statistically significant. Due to the large spatial correlation between variations in [DIV] and *E-P* with ENSO, only [DIV] is shown.

Table 1. Coefficients, r^2 Values, Mean Square Error (MSE), and F Statistics for Three Linear Regression Models Predicting the Change in CAM δD_q With ENSO ($\Delta\delta D_q$)[a]

Model	b_1	b_2	r^2	MSE	F
$b_1\Delta$[DIV]	6.73 (0.20)	---	0.44	81	1184
$b_1\Delta P$	−7.14 (0.24)	---	0.37	91	883
$b_1\Delta P + b_2\Delta E$	−6.55 (0.23)	7.28 (0.46)	0.45	79	635

[a]Δ[DIV] is the change in CAM vertically integrated moisture flux divergence with ENSO, ΔP is the change in CAM precipitation with ENSO, and ΔE is the change in CAM evaporation with ENSO. All coefficients (b_1, b_2) and F statistics are characterized by $p < 0.05$. The standard error associated with each coefficient estimate is shown in parentheses.

of δD_q to isolate the isotopic signal associated with shifts between *E*- and *P*-dominated environments.

Nevertheless, an important concern with the δD_q estimates from satellite is that very few of the individual grid points in the composite difference patterns are statistically significant (Figure 6a). This is largely an effect of small sample sizes: the median n, or days of observational coverage for a single 3° × 3° grid box during each ENSO phase, is 34. To identify significant isotopic differences between ENSO phases, it is thus necessary to boost the TES sample size by averaging over larger geographic areas.

Figure 7 presents the differences in mean conditions between cold and warm phases of ENSO averaged over the five boxed regions shown in Figures 3 and 6. Three important results emerge. First, TES δD_q always changes in the same direction as [DIV], and these changes are significant in all regions but box 3. Changes in δD_z, in contrast, are not always of the same sign, supporting the idea that δD_z is not a reliable tracer of *E-P* like δD_q. Second, the observations are consistent with the CAM output, which shows significant changes in δD_q across all five regions. Third, δD_q changes significantly with [DIV] even when there is no significant regional change in *P* (e.g., box 5)—another indication that δD_q responds to the balance between *E* and *P* and not just to *P* alone.

Moreover, even though composite differences in δD_q may be insignificant at most grid points, the spatial correlation of these differences with [DIV] is highly significant. As reported in Table 1, a simple linear regression explains 43.7% of the variance in the δD_q composite difference pattern and suggests that a 1 mm day^{-1} increase in [DIV] causes a 6.73 ± 0.20‰ change in δD_q. To exclude outliers, the model is fit only to those grid points where the differences in δD_q, [DIV], *E*, and *P* do not exceed a distance 1.5 times the interquartile range beyond their respective upper and lower quartile values (Figure 8). Both the estimated slope of the line and the regression itself are highly significant ($p \ll .001$). Regressing the change in δD_q on both *E* and *P* using the same truncated data set (n = 1527, compared to 1702 tropical oceanic grid points with finite [DIV] values) explains a similar amount of variance. In contrast, while regressing the change in δD_q on the change in *P* produces both a significant slope and a significant fit, the variance explained is lower and the mean square error larger. Thus, even though changes in evaporation with ENSO are small, they appear to play a significant role in altering regional moisture imbalances and shaping the isotopic composition of free tropospheric water vapor.

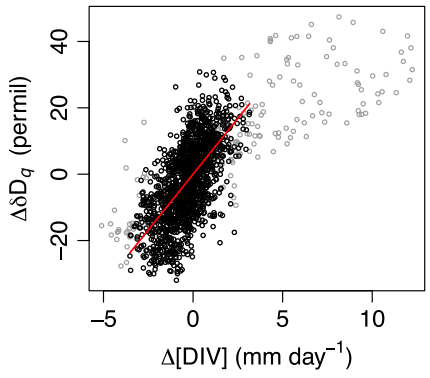

Figure 8. Regression of the CAM δD_q composite difference pattern of Figure 6b ($\Delta\delta D_q$) on the CAM [DIV] composite difference pattern shown in Figure 5b (Δ[DIV]). The regression tests the spatial dependence of changes in δD_q on changes in [DIV] between cold and warm phases of ENSO. Grid points included in the regression model (red line) are shown in black and described in the text. Model statistics are reported in Table 1.

3.3. Evaluating the Sensitivity of δD_q to *E-P*

While section 3.2 provides strong evidence that changes in δD_q are highly correlated with shifting regional moisture imbalances associated with ENSO, it remains to be shown whether the changes in [DIV]—our proxy for *E-P*—are indeed the cause of the variations in δD_q. If so, one might reasonably assume that δD_q should covary with [DIV] irrespective of the strength or phase of ENSO, as well as while *P* remains essentially

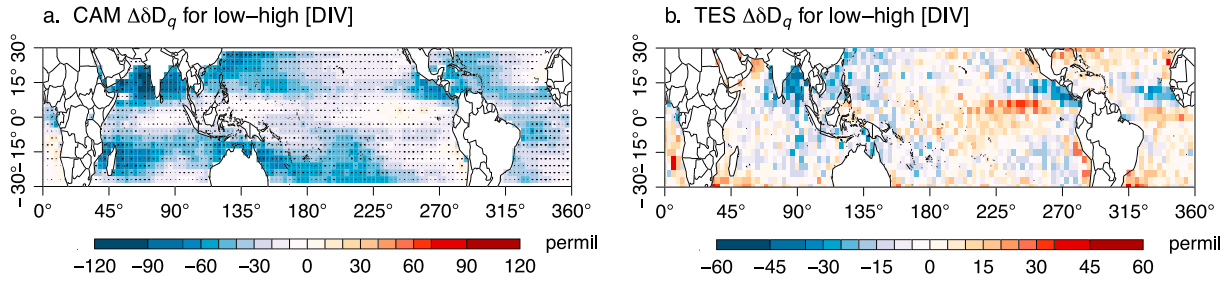

Figure 9. Composite differences in (a) CAM and (b) TES δD_q for periods of low and high [DIV], irrespective of the phase or strength of ENSO. Stippling in Figure 9a indicates significant differences. As described in section 2, low and high periods are defined at a particular grid point by days in which CAM (Figure 9a) or ERA (Figure 9b) [DIV] is in the bottom or top quartile of its distribution for the full September 2004 to December 2011 analysis period. Equivalent composite differences in δD_q for periods of low and high *E-P* are provided in the supporting information. Note that the scale for the TES composite difference is half the scale of the CAM composite difference.

constant. To test these suppositions, composite differences in δD_q are computed for periods of low and high [DIV] at each grid point for the entire September 2004 to December 2011 period and for periods when *P* falls within the following narrow precipitation bins: 0–1 mm day^{-1}, 1–2.5 mm day^{-1}, 2.5–5 mm day^{-1}, and 5+ mm day^{-1} (section 2.3 provides a complete description of the methods). Equivalent composite differences for periods of low and high *E-P* are provided for reference in the supporting information to show that the steady state assumption of equation (1) is still reasonable despite the fact that binning accentuates higher frequency variability in moisture fluxes and moisture flux divergence.

Starting with the composite differences in δD_q for periods of low and high [DIV], Figure 9a suggests that CAM δD_q decreases at most grid points as [DIV] decreases, regardless of the strength or phase of ENSO. More than 96% of tropical oceanic grid points exhibit a negative change in δD_q, and 97.7% of these are significant. While the magnitude of the change is quite small in the subtropical stratocumulus regions and along the equatorial convergence zones, modeled [DIV] also varies little on average in these regions. Only the eastern Pacific is characterized by largely insignificant changes.

Differences in TES δD_q (Figure 9b), in comparison, show much weaker sensitivity to variations in [DIV] and are largely insignificant, likely reflecting both limited temporal coverage and instrumental and retrieval uncertainties in the remotely sensed data product. One key consideration, for example, is that because TES retrievals near raining clouds are excluded from the analysis, the low [DIV] composite is probably composed of observations taken in low-fractional cloud cover pockets in which [DIV] likely differs from the grid-averaged conditions. This becomes more critical a concern when assessing shorter-term variations in convective activity as compared to long-duration changes associated with ENSO. Nevertheless, similar to CAM, TES δD_q decreases as [DIV] decreases in most tropical oceanic regions except the eastern Pacific. There the TES composite difference shows a noticeable increase in δD_q, which suggests that other factors may influence the isotopic variability of this region on shorter time scales.

Figure 10 shows the CAM δD_q composite differences recalculated for low and high [DIV] when *P* also falls within narrow prescribed ranges. Scatterplots (not shown) confirm that binning the model output in this manner eliminates the co-dependence of [DIV] and *P*, except for the highest precipitation bin (e.g., 5+ mm day^{-1}). However, it also greatly reduces the sample sizes for certain statistical comparisons. For example, in the subtropical stratocumulus regions, where [DIV] is strongly positive (Figure 1b), *P* is almost always low. Therefore, few days are simulated in which $P > 1$ mm day^{-1}. Similarly, along the Intertropical Convergence Zone (ITCZ), where [DIV] is strongly negative (Figure 1b), *P* is seldom less than 1 mm day^{-1}. Consequently, one would not expect to see significant differences in δD_q in these regions for all precipitation bins. These concerns notwithstanding, Figure 10 clearly reveals that at the vast majority of grid points, δD_q decreases significantly when [DIV] also decreases, even while *P* is relatively constant. This finding confirms that δD_q traces the column-average hydrologic balance and not just *P* alone. The exception to this pattern is—once again—the equatorial eastern Pacific, where a number of significant changes in δD_q are anticorrelated with [DIV] (Figures 10a–10c), indicating that additional controls must be considered on the shorter time scales on which mesoscale features that induce convective activity exist.

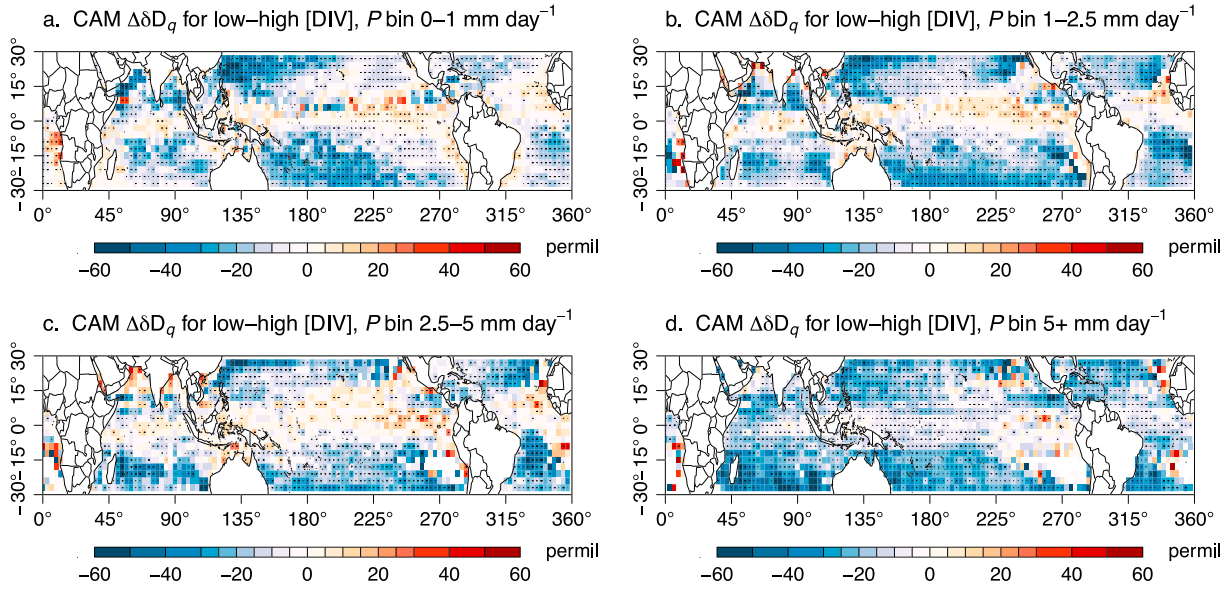

Figure 10. Changes in δD_q with [DIV] when P is held constant. Composite differences in CAM δD_q for periods when [DIV] is in the bottom or top quartile of its distribution at each grid point and P falls within the following precipitation bins: (a) 0–1 mm day^{-1}, (b) 1–2.5 mm day^{-1}, (c) 2.5–5 mm day^{-1}, and (d) 5+ mm day^{-1}. Stippling indicates significant differences. Equivalent composite differences in δD_q for periods of low and high E-P are provided in the supporting information.

4. Discussion

This study develops a new metric—δD_q—to track shifting regional moisture imbalances between E and P, represented by changes in [DIV] (equation (1)). The analysis shows that over the tropical oceanic region spanning 30°S–30°N, changes in δD_q with ENSO are strongly spatially correlated with changes in [DIV]. A sensitivity test further shows that outside the equatorial eastern Pacific, these correlations persist on shorter time scales, even when P remains constant. This section discusses first why δD_q succeeds as a tracer of E-P when more traditional isotopic metrics such as δD_z do not, then the limitations of estimating δD_q from satellite observations, and last the implications of using δD_q to monitor hydroclimate variability.

4.1. Understanding Why δD_q Traces E-P

A key finding of this analysis is that the water vapor isotope ratio traces E-P when normalized to a reference water vapor concentration. The reason for this may be understood by revisiting Figure 2. Regardless of whether an environment is dominated by E (blue line) or P (red line), to first order, the isotope ratio (δD) covaries with the water vapor volume mixing ratio (q). Consequently, variations in specific humidity may cause isotopic variations that easily dwarf any signal associated with shifting hydrological processes. By normalizing the isotope ratio with respect to water vapor concentration, δD_q isolates the portion of isotopic variability most closely associated with the shift between E- and P-dominated regimes.

Figure 11 emphasizes this point by showing mean water vapor volume mixing ratio (q, Figure 11a) and water vapor δD (Figure 11b) profiles from CAM binned by E-P. The bins are defined by E-P values of −7.5 to −4.5 mm day^{-1}, −3.0 to −1.5 mm day^{-1}, 0.5 to 1.5 mm day^{-1}, and 3.0 to 4.5 mm day^{-1}, using the daily mean model output from all tropical oceanic grid points for the entire September 2004 to December 2011 analysis period. Figure 11b shows that when δD is plotted as a function of height, the four profiles are nearly indistinguishable, particularly at lower altitudes. However, when δD is plotted as a function of q (Figure 11c), clear differences emerge: for a given water vapor concentration, the vapor is systematically depleted as E-P decreases, or P becomes dominant. These differences are accentuated at lower humidity values due to the curvature of the bivariate distributions. Isotopic variations around a reference water vapor concentration are thus more effective than isotopic variations around a reference altitude in distinguishing E- and P-dominated regimes.

To understand the physical reasons why δD_q traces [DIV], it is convenient to think of E-P as representing a simple balance between isotopically enriching and depleting processes (Figure 2). Accordingly, regions

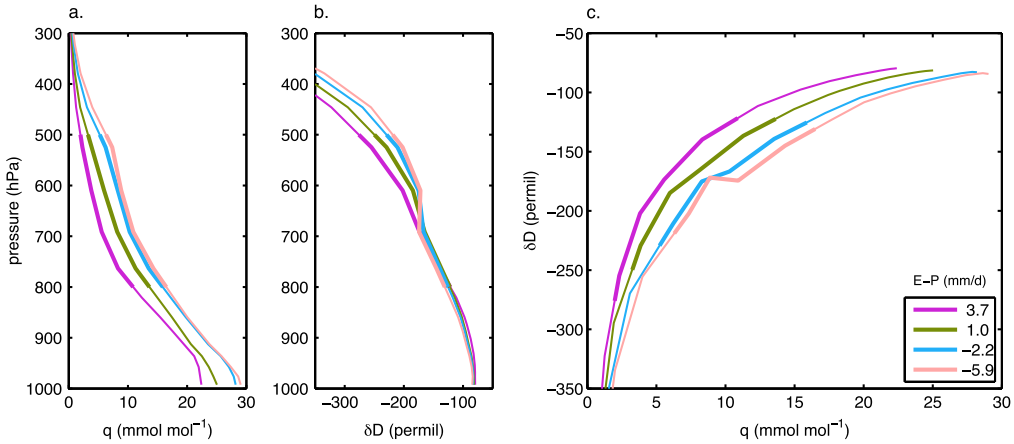

Figure 11. Comparison of isotopic variations around a reference pressure and isotopic variations around a reference water vapor volume mixing ratio for distinct bins of *E-P*. Mean simulated profiles of (a) water vapor volume mixing ratio (q) and (b) the water vapor isotope ratio (δD) as a function of pressure. (c) Simulated δD shown as a function of q. The curves are smoothed composites representing *E-P* bins of -7.5 to -4.5 mm day^{-1} (light pink), -3.0 to -1.5 mm day^{-1} (blue), 0.5 to 1.5 mm day^{-1} (green), and 3.0 to 4.5 mm day^{-1} (purple), using the daily mean CAM output from all tropical oceanic grid points for the entire September 2004 to December 2011 analysis period. Thicker line widths identify the 800–500 hPa layer of the atmosphere. Isotopic variations around a reference q of 4 mmol mol^{-1} are clearly much more distinguishable than isotopic variations around a fixed height.

dominated by precipitation should be much more depleted at the same water vapor volume mixing ratio than regions dominated by evaporation. Since *P*-dominated regions are characterized by negative [DIV] while *E*-dominated regions are characterized by positive [DIV] (Figure 1), δD_q and [DIV] should, as a result, be correlated.

However, this simplistic argument likely neglects the important fact that the moisture transport required to sustain precipitation in regions where $P > E$ also plays a role in shaping the isotopic composition of the free troposphere. For example, *Moore et al*. [2014] argued that when convection intensifies and the layer of convergence deepens, the moisture entrained into the convective column from the surrounding region becomes more depleted (since the isotope ratio tends to decrease with height in the lower troposphere and midtroposphere). They applied this argument to explain why precipitation isotope ratios decrease when the contribution of imported moisture to local precipitation increases. Recent work by *Torri et al*. [2017] substantiates their claims by showing that the isotopic composition of precipitation decreases when the mean level of convergence increases, even if the precipitation rate remains constant.

Since well-developed convection is characterized by strong midlevel inflow [*Houze*, 2004], it is tempting to assume that increasing convective activity always results in the convergence of relatively depleted water vapor (not just higher precipitation rates), maintaining a lower δD_q. The δD_q. composite difference patterns observed and simulated for cold and warm phases of ENSO are certainly consistent with this supposition even if they do not evaluate its merits directly. Nevertheless, based on *Torri et al.*'s [2017] findings, it is plausible that if the mean level of moisture entrained decreases while total column convergence increases, then the isotope ratio of water vapor in the convective column could become higher. This might help explain the significant anomalous changes in δD_q found in the east Pacific for the low–high [DIV] composite difference patterns (Figures 9 and 10). After all, the east Pacific is a region where bottom-heavy vertical velocity profiles maintain a low mean level of moisture entrainment even when convection intensifies [*Back and Bretherton*, 2006; *Torri et al*., 2017].

Of course, other factors may confound the relationship between δD_q and [DIV] on the shorter time scales emphasized by the low–high [DIV] composite difference plots (Figures 9 and 10). For example, short-term variations in moisture storage may violate the assumption that [DIV] balances *E-P* (equation (1)); however, composite difference in δD_q for periods of low and high *E-P* (see supporting information) are sufficiently similar to the composite differences for periods of low and high [DIV] to negate this claim. Another possibility is that vapor recycling at low levels and postcondensational processes, such as rain reevaporation, significantly

influence the isotope ratios of water vapor and precipitation in convection without altering the humidity greatly [e.g., *Risi et al*., 2008; *Wright et al*., 2009; Kurita, 2013]. Yet these effects tend to reinforce the isotopic depletion expected with greater convergence as precipitation intensifies. Large-scale advection could also play a role by shifting the isotopic trace of convection to areas "downstream" [e.g., Gedzelman, 1988; *Galewsky et al*., 2007; *Hurley et al*., 2012; *Bailey et al*., 2013], though whether this would sufficiently obfuscate the correlation between δD_q and [DIV] at a particular location is unclear. Finally, variations in SST may have a sufficiently strong enriching effect on boundary layer water vapor that δD_q could increase even while convective invigoration causes [DIV] to decrease (see Figure 2 for reference). This last effect might be particularly relevant in the east Pacific, since convergence is strongly linked to SST gradients there [*Back and Bretherton*, 2009].

With dramatic changes in SST a hallmark of ENSO, an obvious question is whether sea surface variations could also confound the relationship between δD_q and [DIV] over longer seasonal averages. Most evidence points to the contrary. First, differences in δD_q for cold and warm phases of ENSO are clearly much more closely aligned with variations in convective activity (Figure 3) and [DIV] (Figures 4b and 5b) than with canonical patterns of SST change [e.g., *Trenberth and Caron*, 2000] (Figure 3d). Second, normalizing δD_q by the prediction from a Rayleigh model [cf. *Samuels-Crow et al*., 2014] largely accounts for differences in boundary layer conditions between ENSO phases (see supporting information for a more detailed discussion); yet such normalization does not change the spatial patterns shown in Figures 6a and 6b qualitatively. Third, the east Pacific, which exhibits anomalous anticorrelations between δD_q and [DIV] on shorter time scales (Figures 9 and 10), shows the expected positive correlation between δD_q and [DIV] across ENSO phases. These results suggest that water vapor isotope ratios robustly trace shifting regional moisture imbalances even when substantive changes in SST occur. Nevertheless, TES does fail to detect significant changes in δD_q between ENSO phases in the central Pacific (box 3, Figures 6a and 7a)—a region of strong SST (Figure 3d) changes during El Niño. The importance of SST in modifying the δD_q-[DIV] relationship is therefore deserving of further exploration.

4.2. Limitations of Estimating δD_q From Remote Sensing

In addition to being a natural tracer of the hydrological cycle, one advantage of using δD_q to track *E-P* is that it can be derived from remote sensing observations, which provide information on a near-global scale during both rainy and dry conditions. However, TES's spatiotemporal coverage is limited by the need to eliminate all retrievals but those with the lowest fractional cloud coverage. Thus, while the δD_q composite differences estimated from TES are broadly consistent with the model simulations from CAM, the observed changes in δD_q are much less spatially coherent and are seldom statistically significant at individual locations.

Averaging over large spatial domains (e.g., Figure 7) is one way to circumvent the problem of small n in the absence of longer time series data. However, even such averaging techniques cannot improve the significance of the observations in all regions. For instance, over the central Pacific—the principal region of El Niño convective activity—TES does not detect a significant change in δD_q between cold and warm phases of ENSO, even when the isotopic data are averaged over a 15° × 25° area (box 3, Figure 7a). These findings suggest that while remotely sensed isotope ratios are powerful tools for detecting broad patterns of regional hydrological change, they may not be as effective at monitoring changes within individual regions. Fortunately, growing networks of in situ water vapor measurements are opening the door for monitoring local hydrological changes with much greater accuracy [*Galewsky et al*., 2016]. The challenge for these measurements will be in designing sampling systems that can maximize exposure to free tropospheric air in order to achieve sufficiently large observational footprints.

4.3. Implications for Monitoring Hydroclimate Variability

Much of the motivation for developing a metric like δD_q stems from the expectation that greenhouse-gas forcing will cause significant changes to the global water cycle [*Held and Soden*, 2006]. Growing disparities in *E-P* regionally are expected to widen the distance between moisture sources and sinks, essentially altering the hydrological links that connect one region to another [*Singh et al*., 2016]. Although satellite observations of tropical precipitation provide indirect evidence of recent water cycle intensification [*John et al*., 2009; *Allan et al*., 2010; *Li et al*., 2011; *Zhou et al*., 2011], there remains disagreement over how much the water cycle will respond to warming, hence the value in developing a new, independent and observationally based metric

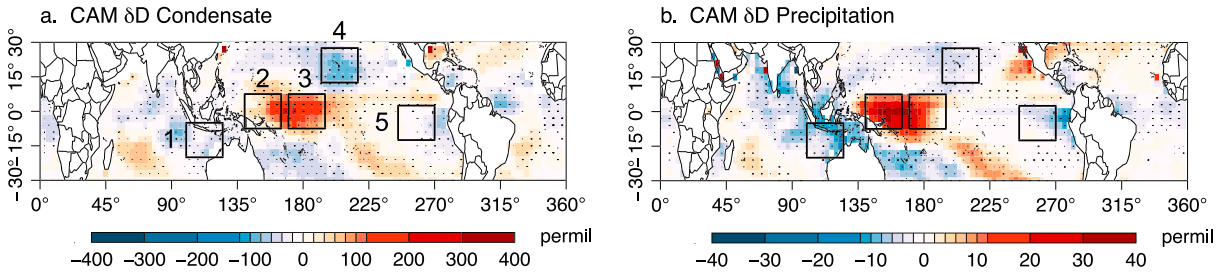

Figure 12. Composite differences in the δD of (a) total column condensate and (b) precipitation, estimated from CAM, for cold minus warm phases of ENSO. Stippling indicates significant differences. The five boxed regions are the same as those shown in Figure 3 and discussed in the text.

that it is sensitive not just to *P* but to the balance of *E* and *P* and that can trace shifting regional moisture imbalances robustly.

In addition to providing a tool for monitoring future changes in the hydrological cycle, this study also has important implications for how we interpret the hydroclimate of the past. *Lee et al.* [2007] and *Moore et al.* [2014], for instance, argued that the same column average hydrologic balance that controls the isotopic composition of water vapor also controls the isotopic composition of precipitation. Figure 12 provides additional evidence for this claim by showing composite differences in the isotopic composition of CAM total column condensate and precipitation for distinct phases of ENSO. Because the isotope ratios of condensate and precipitation are weighted by the liquid water volume mixing ratio, they are essentially normalized in much the same way as δD_q is normalized to a reference water vapor concentration. Figures 12a and 12b mirror the δD_q composite differences between La Niña and El Niño periods shown earlier (Figure 6b), indicating that cloud and precipitation isotopic changes are also spatially correlated with the variations in regional moisture imbalances that result from large-scale convective reorganization. With precipitation isotopic measurements from the Global Network of Isotopes in Precipitation (GNIP) dating back to the 1950s, Figure 12 suggests that it should be possible to investigate changes in *E-P* over a much longer time span than the satellite record, albeit at a significantly reduced number of locations. Moreover, since precipitation isotope ratios shape many isotopic proxy records used to infer past climate, tropical paleoproxies should provide a record of *E-P* over a substantially longer period.

This idea—that the balance of *E-P* is what controls tropical precipitation isotope ratios—differs from traditional views that precipitation isotope ratios are indicators of local precipitation intensity or amount [e.g., *Dansgaard*, 1964; *Cruz et al.*, 2005; *Tierney et al.*, 2008; *Niedermeyer et al.*, 2010; *Sano et al.*, 2012]. Although appearing widely in the literature, the latter has proven problematic since the exact relationship between local precipitation isotope ratios and precipitation amount varies substantially across tropical locations [*Kurita*, 2013; *Lekshmy et al.*, 2014]. It is also statistically insignificant at many sites on time scales shorter than 1 month [*Kurita et al.*, 2009; *Conroy et al.*, 2016]—a puzzling finding given that both precipitation rate and isotope ratios vary dramatically over the lifetime of individual storms [*Coplen et al.*, 2008; *Good et al.*, 2014]. By demonstrating that changes in regional moisture imbalances (e.g., *E-P*) can explain water isotopic variations, even in the absence of significant changes in precipitation, this study provides a more unifying theoretical framework for interpreting the relationship between water isotope ratios and precipitation. Furthermore, it supports a growing body of work that suggests that isotopic information in modern and paleoprecipitation records can be used to interpret changes in the organization of large-scale convection [*Cobb et al.*, 2007; *Kurita et al.*, 2009; *Kurita*, 2013; *Moerman et al.*, 2013; *Lekshmy et al.*, 2014; *Samuels-Crow et al.*, 2014; *Sutanto et al.*, 2015; *Aggarwal et al.*, 2016].

5. Summary

As climate warms, regional differences in evaporation and precipitation are likely to become more disparate, causing the drier *E*-dominated regions of the tropics to become drier and the wetter *P*-dominated regions to become wetter [*Held and Soden*, 2006]. Satellite observations of recent changes in tropical precipitation support these predictions [*John et al.*, 2009; *Allan et al.*, 2010; *Li et al.*, 2011; *Zhou et al.*, 2011], as do in situ measurements of changes in ocean salinity [*Helm et al.*, 2010; *Durack et al.*, 2012]. However, little consensus exists as to just how much the hydrological cycle has intensified already or how much it will intensify in the future.

This study presents a new metric for identifying regional imbalances in *E* and *P* using the isotope ratio of water vapor normalized to a reference water vapor concentration of 4 mmol mol^{-1} (i.e., δD_q). The new metric is derived both from remote sensing observations and from an isotopically enabled general circulation model.

To evaluate the performance of δD_q, composite differences between cold and warm phases of ENSO are compared with composite differences in [DIV], under the assumption that [DIV] balances *E-P* when changes in moisture storage are negligible. The comparisons show that δD_q tracks shifting regional moisture imbalances, even if the amount of precipitation changes little or not at all. The analysis further examines composite differences in δD_q for low and high periods of [DIV], irrespective of the strength or phase of ENSO and while holding precipitation constant. Even though binning by precipitation accentuates higher frequency variability in moisture fluxes and moisture flux divergence, simulated δD_q and [DIV] continue to show significant positive correlations in most regions. These results confirm that δD_q is indeed a tracer of *E-P* and not just *P* alone. The eastern equatorial Pacific is an exception to this pattern. There additional factors such as the mean level of moisture convergence or SST gradients may confound the δD_q-[DIV] correlation on shorter time scales. Since the isotopic signature of *E-P* in water vapor transfers to the isotope ratios of condensate and precipitation, the results of this work suggest that water isotope ratios should serve as powerful tracers of past and future climate variability.

Acknowledgments

A. Bailey thanks the Joint Institute for the Study of the Atmosphere and Ocean for a postdoctoral research fellowship that supported this research, H. Singh at the University of Washington for numerous thought-provoking discussions on hydroclimate variability, and the manuscript's reviewers for their in-depth and thoughtful critiques. P. Blossey and D. Noone were supported by the NASA Modeling, Analysis and Prediction Program through grant NNX13AN47G. J. Nusbaumer and the development of the isotopic version of CAM were supported by the NSF Paleoclimate program (AGS-1049104) and Climate and Large Scale Dynamics program as part of a Faculty Early Career Development award (AGS-0955841) and made use of computing resources provided by the Climate Simulation Laboratory at the National Center for Atmospheric Research's Computational and Information Systems Laboratory, sponsored by the National Science Foundation. Data used in this analysis may be located via the references and websites cited in the main text.

References

Aggarwal, P. K., U. Romatschke, L. Araguas-Araguas, D. Belachew, F. J. Longstaffe, P. Berg, C. Schumacher, and A. Funk (2016), Proportions of convective and stratiform precipitation revealed in water isotope ratios, *Nat. Geosci.*, *9*, 624–629, doi:10.1038/ngeo2739.

Allan, R. P., B. J. Soden, V. O. John, W. Ingram, and P. Good (2010), Current changes in tropical precipitation, *Environ. Res. Lett.*, *5*, 025205, doi:10.1088/1748-9326/5/2/025205.

Back, L. E., and C. S. Bretherton (2006), Geographic variability in the export of moist static energy and vertical motion profiles in the tropical Pacific, *Geophys. Res. Lett.*, *33*, L17810, doi:10.1029/2006GL026672.

Back, L. E., and C. S. Bretherton (2009), On the relationship between SST gradients, boundary layer winds, and convergence over the tropical oceans, *J. Clim.*, *22*, 4182–4196, doi:10.1175/2009JCLI2392.1.

Bailey, A., D. Toohey, and D. Noone (2013), Characterizing moisture exchange between the Hawaiian convective boundary layer and free troposphere using stable isotopes in water, *J. Geophys. Res. Atmos.*, *118*, 8208–8221, doi:10.1002/jgrd.50639.

Bailey, A. (2014), Evaluating shallow convective mixing and precipitation processes using isotope ratios in water vapor, PhD thesis, Dep. of Atmos. Ocean. Sci., Univ. of Colo. Boulder, Boulder.

Bailey, A., J. Nusbaumer, and D. Noone (2015), Precipitation efficiency derived from isotope ratios in water vapor distinguishes dynamical and microphysical influences on subtropical atmospheric constituents, *J. Geophys. Res. Atmos.*, *120*, 9119–9137, doi:10.1002/2015JD023403.

Berkelhammer, M., C. Risi, N. Kurita, and D. Noone (2012), The moisture source sequence for the Madden-Julian Oscillation as derived from satellite retrievals of HDO and H_2O, *J. Geophys. Res.*, *117*, D03106, doi:10.1029/2011JD016803.

Brown, D., J. Worden, and D. Noone (2008), Comparison of atmospheric hydrology over convective continental regions using water vapor isotope measurements from space, *J. Geophys. Res.*, *113*, D15124, doi:10.1029/2007JD009676.

Brown, D., J. Worden, and D. Noone (2013), Characteristics of tropical and subtropical atmospheric moistening derived from Lagrangian mass balance constrained by measurements of HDO and H_2O, *J. Geophys. Res. Atmos.*, *118*, 54–72, doi:10.1029/2012JD018507.

Cobb, K. M., J. F. Adkins, J. W. Partin, and B. Clark (2007), Regional-scale climate influences on temporal variations of rainwater and cave dripwater oxygen isotopes in northern Borneo, *Earth Planet. Sci. Lett.*, *263*, 207–220, doi:10.1016/j.epsl.2007.08.024.

Conroy, J. L., D. Noone, K. M. Cobb, J. W. Moerman, and B. L. Konecky (2016), Paired stable isotopologues in precipitation and vapor: A case study within western tropical Pacific storms, *J. Geophys. Res. Atmos.*, *121*, 3290–3303, doi:10.1002/2015JD023844.

Coplen, T. B., P. J. Neiman, A. B. White, J. M. Landwehr, F. M. Ralph, and M. D. Dettinger (2008), Extreme changes in the stable hydrogen isotopes and precipitation characteristics in a landfalling Pacific storm, *Geophys. Res. Lett.*, *21*, L21808, doi:10.1029/2008GL035481.

Cruz, F. W., Jr., S. J. Burns, I. Karmann, W. D. Sharp, M. Vuille, A. O. Cardoso, J. A. Ferrari, P. L. Silva Dias, and O. Viana Jr. (2005), Insolation-driven changes in atmospheric circulation over the past 116,000 years in subtropical Brazil, *Nature*, *434*, 63–66, doi:10.1038/nature03365.

Dansgaard, W. (1964), Stable isotopes in precipitation, *Tellus*, *16*, 436–468.

Dee, D. P., et al. (2011), The ERA-Interim reanalysis: Configuration and performance of the data assimilation system, *Q.J.R, Meteorol. Soc.*, *137*, 553–597, doi:10.1002/qj.828.

Durack, P. J. S., E. Wijffels, and R. J. Matear (2012), Ocean salinities reveal strong global water cycle intensification during 1950 to 2000, *Science*, *336*, 455–458, doi:10.1126/science.1212222.

Galewsky, J., M. Strong, and Z. D. Sharp (2007), Measurements of water vapor *D/H* ratios from Mauna Kea, Hawaii, and implications for subtropical humidity dynamics, *Geophys. Res. Lett.*, *34*, L22808, doi:10.1029/2007GL031330.

Galewsky, J., H. C. Steen-Larsen, R. D. Field, J. Worden, C. Risi, and M. Schneider (2016), Stable isotopes in atmospheric water vapor and applications to the hydrologic cycle, *Rev. Geophys.*, *54*, 809–865, doi:10.1002/2015RG000512.

Gat, J. R. (1996), Oxygen and hydrogen isotopes in the hydrologic cycle, *Annu. Rev. Earth Planet. Sci.*, *24*, 225–262.

Gedzelman, S. D. (1988), Deuterium in water vapor above the atmospheric boundary layer, *Tellus*, *40B*, 134–147.

Gill, A. E., and E. M. Rasmusson (1983), The 1982–83 climate anomaly in the equatorial Pacific, *Nature*, *306*, 229–234.

Good, S. P., D. V. Mallia, J. C. Lin, and G. J. Bowen (2014), Stable isotope analysis of precipitation samples obtained via crowdsourcing reveals the spatiotemporal evolution of Superstorm Sandy, *PLoS One*, *9*, e91117, doi:10.1371/journal.pone.0091117.

Held, I. M., and B. J. Soden (2006), Robust responses of the hydrological cycle to global warming, *J. Clim.*, *19*, 5686–5699.

Helm, K. P., N. L. Bindoff, and J. A. Church (2010), Changes in the global hydrological-cycle inferred from ocean salinity, *Geophys. Res. Lett.*, *37*, L18701, doi:10.1029/2010GL044222.

Holloway, C. E., and J. D. Neelin (2009), Moisture vertical structure, column water vapor, and tropical deep convection, *J. Atmos. Sci.*, *66*, 1665–1683, doi:10.1175/2008JAS2806.1.

Houze, R. A., Jr. (2004), Mesoscale convective systems, *Rev. Geophys.*, *42*, RG4003, doi:10.1029/2004RG000150.

Hurley, J., J. Galewsky, J. Worden, and D. Noone (2012), A test of the advection-condensation model for subtropical water vapor using stable isotopologue observations from Mauna Loa Observatory, Hawaii, *J. Geophys. Res.*, *117*, D19118, doi:10.1029/2012JD018029.

John, V. O., R. P. Allan, and B. J. Soden (2009), How robust are observed and simulated precipitation responses to tropical ocean warming? *Geophys. Res. Lett.*, *36*, L14702, doi:10.1029/2009GL038276.

Kurita, N. (2013), Water isotopic variability in response to mesoscale convective system over the tropical ocean, *J. Geophys. Res. Atmos.*, *118*, 10,376–10,390, doi:10.1002/jgrd.50754.

Kurita, N., K. Ichiyanagi, J. Matsumoto, M. D. Yamanaka, and T. Ohata (2009), The relationship between the isotopic content of precipitation and the precipitation amount in tropical regions, *J. Geochem. Explor.*, *102*, 113–122, doi:10.1016/j.gexplo.2009.03.002.

Lee, J., J. Worden, D. Noone, K. Bowman, A. Eldering, A. LeGrande, J.-L. F. Li, G. Schmidt, and H. Sodemann (2011), Relating tropical ocean clouds to moist processes using water vapor isotope measurements, *Atmos. Chem. Phys.*, *11*, 741–752, doi:10.5194/acp-11-741-2011.

Lee, J., J. Worden, D. Noone, J. H. Chae, and C. Frankenberg (2015), Isotopic changes due to convective moistening of the lower troposphere associated with variations in the ENSO and IOD from 2005 to 2006, *Tellus B*, *67*, 26177, doi:10.3402/tellusb.v67.26177.

Lee, J.-E., I. Fung, D. J. DePaolo, and C. C. Henning (2007), Analysis of the global distribution of water isotopes using the NCAR atmospheric general circulation model, *J. Geophys. Res.*, *112*, D16306, doi:10.1029/2006JD007657.

Lekshmy, P. R., M. Midhun, R. Ramesh, and R. A. Jani (2014), ^{18}O depletion in monsoon rain relates to large scale organized convection rather than the amount of rainfall, *Sci. Rep.*, *4*, 5661, doi:10.1038/srep05661.

Li, L., X. Jiang, M. T. Chahine, E. T. Olsen, E. J. Fetzer, L. Chen, and Y. L. Yung (2011), The recycling rate of atmospheric moisture over the past two decades (1988–2009), *Environ. Res. Lett.*, *6*, 034018, doi:10.1088/1748-9326/6/3/034018.

Liebmann, B., and C. A. Smith (1996), Description of a complete (interpolated) outgoing longwave radiation dataset, *Bull. Am. Meteorol. Soc.*, *77*, 1275–1277.

Moerman, J. W., K. M. Cobb, J. F. Adkins, H. Sodemann, B. Clark, and A. A. Tuen (2013), Diurnal to interannual rainfall $\delta^{18}O$ variations in northern Borneo driven by regional hydrology, *Earth Planet. Sci. Lett.*, *369-370*, 108–119, doi:10.1016/j.epsl.2013.03.014.

Moore, M., Z. Kuang, and P. N. Blossey (2014), A moisture budget perspective of the amount effect, *Geophys. Res. Lett.*, *41*, 1329–1335, doi:10.1002/2013GL058302.

Niedermeyer, E. M., E. Schefuß, A. L. Sessions, S. Mulitza, G. Mollenhauer, M. Schulz, and G. Wefer (2010), Orbital- and millennial-scale changes in the hydrologic cycle and vegetation in the western African Sahel: Insights from individual plant wax δD and $\delta^{13}C$, *Quat. Sci. Rev.*, *29*, 2996–3005, doi:10.1016/j.quascirev.2010.06.039.

Noone, D. (2012), Pairing measurements of the water vapor isotope ratio with humidity to deduce atmospheric moistening and dehydration in the tropical midtroposphere, *J. Clim.*, *25*, 4476–4494.

Nusbaumer, J., T. Wong, C. Bardeen, and D. Noone (2017), Evaluating hydrological processes in the Community Atmosphere Model Version 5 (CAM5) using stable isotope ratios of water, *J. Adv. Model Earth Syst.*, *9*, doi:10.1002/2016MS000839.

Rasmusson, E. M., and J. M. Wallace (1983), Meteorological aspects of the El Niño/Southern Oscillation, *Science*, *222*, 1195–1202.

Risi, C., S. Bony, and F. Vimeux (2008), Influence of convective processes on the isotopic composition ($\delta^{18}O$ and δD) of precipitation and water vapor in the tropics: 2. Physical interpretation of the amount effect, *J. Geophys. Res.*, *113*, D19306, doi:10.1029/2008JD009943.

Samuels-Crow, K. E., J. Galewsky, D. R. Hardy, Z. D. Sharp, J. Worden, and C. Braun (2014), Upwind convective influences on the isotopic composition of atmospheric water vapor over the tropical Andes, *J. Geophys. Res. Atmos.*, *119*, 7051–7063, doi:10.1002/2014JD021487.

Sano, M., C. Xu, and T. Nakatsuka (2012), A 300-year Vietnam hydroclimate and ENSO variability record reconstructed from tree ring $\delta^{18}O$, *J. Geophys. Res.*, *117*, D12115, doi:10.1029/2012JD017749.

Singh, H., C. Bitz, A. Donohoe, J. Nusbaumer, and D. Noone (2016), A mathematical framework for analysis of water tracers: Part II, Understanding large-scale perturbations in the hydrological cycle due to CO_2 doubling, *J. Clim.*, *29*, 6765–6782, doi:10.1175/JCLI-D-16-0293.1.

Sutanto, S. J., G. Hoffmann, J. Worden, R. A. Scheepmaker, I. Aben, and T. Röckmann (2015), Atmospheric processes governing the changes in water isotopologues during ENSO events from model and satellite measurements, *J. Geophys. Res. Atmos.*, *13*, 6712–6729, doi:10.1002/2015JD023228.

TES Science Team (2013), TES/Aura level 2, HDO Limb, version 6, Hampton, VA, USA: NASA Atmospheric Science Data Center (ASDC), Accessed TES/Aura L2 Deuterium Oxide (HDO) Lite Nadir (TL2HDOLN) data at doi:10.5067/AURA/TES/TL2HDOLN_L2.006.

Tierney, J. E., J. M. Russell, Y. Huang, J. S. Sinninghe Damsté, E. C. Hopmans, and A. S. Cohen (2008), Northern Hemisphere controls on tropical southeast African climate curing the past 60,000 years, *Science*, *322*, 252–255, doi:10.1126/science.1160485.

Torri, G., D. Ma, and Z. Kuang (2017), Stable water isotopes and large-scale vertical motions in the tropics, *J. Geophys. Res. Atmos.*, *122*, 3703–3717, doi:10.1002/2016JD026154.

Trenberth, K. E., and J. M. Caron (2000), The Southern Oscillation revisited: Sea level pressures, surface temperatures, and precipitation, *J. Clim.*, *13*, 4358–4365, doi:10.1175/1520-0442(2000)013<4358:TSORSL>2.0.CO;2.

Waliser, D. E., N. E. Graham, and C. Gautier (1993), Comparison of the highly reflective cloud and outgoing longwave radiation datasets for use in estimating tropical deep convection, *J. Clim.*, *6*, 331–353.

Wilks, D. S. (2016), The stippling shows statistically significant grid points, *Bull. Am. Meteorol. Soc.*, *97*, 2263–2273, doi:10.1175/BAMS-D-15-00267.1.

Worden, J., D. Noone, K. Bowman, and The Tropospheric Emission Spectrometer science team and data contributors (2007), Importance of rain evaporation and continental convection in the tropical water cycle, *Nature*, *445*, 528–532, doi:10.1038/nature05508.

Worden, J., D. Noone, J. Galewsky, A. Bailey, K. Bowman, D. Brown, J. Hurley, S. Kulawik, J. Lee, and M. Strong (2011), Estimate of bias in Aura TES HDO/H_2O profiles from comparison of TES and in situ HDO/H_2O measurements at the Mauna Loa Observatory, *Atmos. Chem. Phys.*, *11*, 4491–4503, doi:10.5194/acp-11-4491-2011.

Worden, J., S. Kulawik, C. Frankenberg, V. Payne, K. Bowman, K. Cady-Peirara, K. Wecht, J.-E. Lee, and D. Noone (2012), Profiles of CH_4, HDO, H_2O, and N_2O with improved lower tropospheric vertical resolution from Aura TES radiances, *Atmos. Meas. Tech.*, *5*, 397–411, doi:10.5194/amt-5-397-2012.

Wright, J. S., A. H. Sobel, and G. A. Schmidt (2009), Influence of condensate evaporation on water vapor and its stable isotopes in a GCM, *Geophys. Res. Lett.*, *36*, L12804, doi:10.1029/2009GL038091.

Zhou, Y. P., K.-M. Xu, Y. C. Sud, and A. K. Betts (2011), Recent trends of the tropical hydrological cycle inferred from Global Precipitation Climatology Project and International Satellite Cloud Climatology Project data, *J. Geophys. Res.*, *116*, D09101, doi:10.1029/2010JD015197.